NEURAL REGENERATION RESEARCH
www.nrronline.org

Research Article

Intrathecal liproxstatin-1 delivery inhibits ferroptosis and attenuates mechanical and thermal hypersensitivities in rats with complete Freund's adjuvant-induced inflammatory pain

Yi-Fan Deng[1], Ping Xiang[2], Jing-Yi Du[1], Jian-Fen Liang[1], Xiang Li[1, *]

https://doi.org/10.4103/1673-5374.346547
Date of submission: January 12, 2022
Date of decision: March 24, 2022
Date of acceptance: April 18, 2022
Date of web publication: July 1, 2022

From the Contents

Introduction	456
Methods	457
Results	458
Discussion	459

Graphical Abstract

Anti-ferroptosis effects of liproxstatin-1 on CFA-induced inflammatory pain pathology

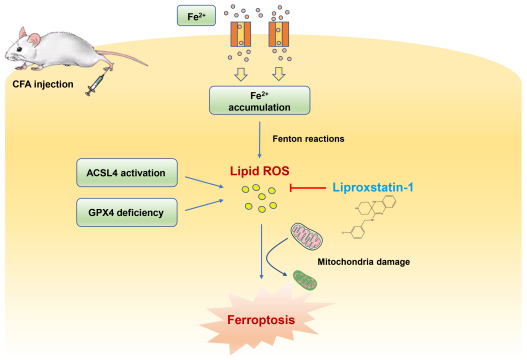

Abstract

Previous studies have confirmed the relationship between iron-dependent ferroptosis and a peripheral nerve injury-induced neuropathic pain model. However, the role of ferroptosis in inflammatory pain remains inconclusive. Therefore, we aimed to explore whether ferroptosis in the spinal cord and dorsal root ganglion contributes to complete Freund's adjuvant (CFA)-induced painful behaviors in rats. Our results revealed that various biochemical and morphological changes were associated with ferroptosis in the spinal cord and dorsal root ganglion tissues of CFA rats. These changes included iron overload, enhanced lipid peroxidation, disorders of anti-acyl-coenzyme A synthetase long-chain family member 4 and glutathione peroxidase 4 levels, and abnormal morphological changes in mitochondria. Intrathecal treatment of liproxstatin-1 (a ferroptosis inhibitor) reversed these ferroptosis-related changes and alleviated mechanical and thermal hypersensitivities in CFA rats. Our study demonstrated the occurrence of ferroptosis in the spinal cord and dorsal root ganglion tissues in a rodent model of inflammatory pain and indicated that intrathecal administration of ferroptosis inhibitors, such as liproxstatin-1, is a potential therapeutic strategy for treating inflammatory pain.

Key Words: cell death; complete Freund's adjuvant; dorsal root ganglion; ferroptosis; inflammatory pain; intrathecal delivery liproxstatin-1; spinal cord

Introduction

Inflammatory pain is a significant form of chronic pain that has become a major health problem and is primarily caused by trauma, arthritis, or pathogen infection, which can lead to allodynia, hyperalgesia, or even cognitive impairment (Ho et al., 2019). Tissue damage or inflammation may induce the overproduction of multiple pro-inflammatory compounds and dysregulation of pain-related genes, which may act as triggers for the emergence and maintenance of painful behaviors (Fattori et al., 2019). Currently, typical pharmacotherapy for inflammatory pain, such as opioids and cyclooxygenase inhibitors, is limited by partial and side effects (Volkow et al., 2018), and new drugs for inflammatory pain remain unavailable because of the obscure pathogenesis of inflammatory pain.

A cell-death disorder of the nervous system has been implicated in the occurrence of inflammatory pain. For example, peripheral complete Freund's adjuvant (CFA) injection has the potential to promote neuronal apoptosis in the lumbar spinal cord and is a development that is thought to contribute to the imbalance of dorsal horn neuron excitability and eventually result in the enhancement of nociceptive signals and hyperalgesia (Liu et al., 2021). Moreover, the activation of spinal microglia following subcutaneous intraplantar CFA administration may be responsible for increased apoptosis by affecting the function of the phosphatase and tensin homologue deleted on chromosome 10/phosphatidylinositol-3-kinase/protein kinase B (PTEN/PI3K/Akt)-pathway function (Baniasadi et al., 2020). However, understanding the pathogenesis of inflammatory pain is complicated by the diverse forms of cell death, and the principal cell-death pathway that contributes to CFA-induced hyperalgesia remains unclear.

Ferroptosis is considered a unique oxidative and iron-driven class of programmed cell death because it does not commonly exhibit morphological changes in the nucleus or an enhancement of caspase-3 activity and is largely uninhibited by caspase suppressors; these features distinguish ferroptosis from previously proposed types of cell death (e.g., necrosis, apoptosis, and autophagy) (Dixon et al., 2012; Zhang et al., 2021a). Numerous studies have highlighted the potentially important roles of this iron-dependent mode of cell death in the occurrence and development of nervous system diseases (Tan et al., 2021; Yao et al., 2021). Previous preclinical investigations have reported that peripheral-nerve injury leads to iron overload (Xu et al., 2019), reactive-oxygen-species (ROS) accumulation (Valek et al., 2017), and mitochondrial dysfunction (Bae et al., 2018) in the spinal cord, which are considered crucial factors in ferroptosis induction. Moreover, a distinct set of ferroptosis-related genes, which include glutathione peroxidase 4 (GPX4), and anti-acyl-CoA synthetase long-chain family member 4 (ACSL4), has been found to be dysregulated in a neuropathic pain model (Guo et al., 2021; Wang et al., 2021). Using a high-throughput sequencing method, a recent study

[1]Department of Anesthesiology, The Third Affiliated Hospital, Sun Yat-sen University, Guangzhou, Guangdong Province, China; [2]Department of Medical Quality Management, Nanfang Hospital, Southern Medical University, Guangzhou, Guangdong Province, China
*Correspondence to: Xiang Li, PhD, lixiang27@mail.sysu.edu.cn.
https://orcid.org/0000-0003-4997-9339 (Xiang Li)

Funding: *This work was supported by the Basic and Applied Basic Research Foundation of Guangdong Province, No. 2021A1515220081 (to XL).*
How to cite this article: *Deng YF, Xiang P, Du JY, Liang JF, Li X (2023) Intrathecal liproxstatin-1 delivery inhibits ferroptosis and attenuates mechanical and thermal hypersensitivities in rats with complete Freund's adjuvant-induced inflammatory pain. Neural Regen Res 18(2):456-462.*

revealed the potential participation of a group of microRNAs and their target genes in the ferroptosis process (Jia et al., 2021). In addition, intraperitoneal injection of specific ferroptosis inhibitors (e.g., ferrostatin-1 and liproxstatin-1) was shown to suppress ferroptosis and alleviate pain-like behaviors in a chronic sciatic-nerve-constriction pain model (Guo et al., 2021; Wang et al., 2021). Taken together, the above evidence suggests that neuropathic pain is attributed to ferroptosis-like neurocyte death.

The overproduction of ROS, subsequent oxidative stress damage, and lipid peroxidation have been observed previously in a CFA-induced inflammatory-pain model with hyperalgesia pathology (Singh and Vinayak, 2015). In addition, a recent review has reported that excess iron generates a considerable amount of damaging ROS via Fenton or Haber Weiss reactions, which may be involved in the progression of osteoarthritis (Sun et al., 2021). However, whether oxidative damage and iron accumulation lead to ferroptosis has not been demonstrated in inflammatory hyperalgesia. Therefore, we explored whether spinal cord and dorsal root ganglion (DRG) ferroptosis plays a causal role in inflammatory pain induced by CFA administration.

Methods

Experimental animals

Responses to CFA administration between male and female rodents do not differ significantly (Bravo-Hernandez et al., 2016); thus, a total of 65 healthy male adult Sprague-Dawley (SD) rats (specific-pathogen-free [SPF] grade) weighing 180–220 g were recruited from SiPeiFu (Beijing) Biotechnology Co., Ltd (Production license number: SCXK [Jing] 2019-0010, Beijing, China) without any pretreatments. Rats were raised in an SPF environment at the Laboratory Animal Center of South China Agricultural University and housed in individual cages in the same room under standard and suitable conditions (12-hour light/dark cycle; 22 ± 2°C; 40–60% relative humidity) with freely available food (pellet diet) and water. All animal experimental procedures were approved by the Animal Care Committee of the South China Agricultural University (No. 2021d036) on May 15, 2021, and conducted in strict accordance with international laws and National Institutes of Health policies, including the Guide for the Care and Use of Laboratory Animals (eighth edition, 2011). This study is reported in accordance with the Animal Research: Reporting of *In Vivo* Experiments 2.0 guidelines (Percie du Sert et al., 2020).

Intrathecal catheterization

Intrathecal catheter implantation was performed as previously reported (Storkson et al., 1996). Under sufficient anesthetization, maintained with isoflurane (induction concentration: 3–4%, maintenance concentration: 1.5–2.5%; RWD Life Science Co, Shenzhen, Guangdong, China), a sterile polyethylene-10 catheter (0.28 mm inner diameter × 0.61 mm outer diameter) was inserted into the subarachnoid space of the rat through the L4–L5 intervertebral foramen. All incisions and saturation steps were carefully performed by an experienced researcher, and a heating pad was prepared in advance to minimize post-operative pain in the experimental rats. To minimize interference in DRG-tissue collection, we implanted the intrathecal catheter contralateral to the CFA injection side. According to a previously proposed method (Yang et al., 2021), the proper position of intrathecal catheterization was characterized by transient hind-limb paralysis induced by intrathecal lidocaine (2%, 20 μL) delivery following recovery from anesthesia. Before pain model construction, rodents spent 3 days in recovery from intrathecal catheterization surgery (**Figure 1A**).

Chronic inflammatory pain model construction and intrathecal drug delivery

All experimental murine were randomly allocated to the following five groups using a random number table: (a) control (Con, *n* = 15), (b) CFA with liproxstatin-1 (CFA-Lip, *n* = 15), (c) CFA with vehicle (CFA-Veh, *n* = 15), (d) CFA with no drug administration (CFA, *n* = 15), and (e) CFA with minocycline (CFA-Mino, *n* = 5). According to previous studies (Abbadie et al., 1996; Huang et al., 2019), we established an inflammatory pain model via subcutaneous intraplantar administration of 100 μL CFA (F5881, MilliporeSigma, Burlington, MA, USA) into the left hind paw. The control rats received an equivalent injection of saline (0.9%, 100 μL) in the comparable area of the left hind paw.

Liproxstatin-1 is the first *in vivo* efficacious ferroptosis inhibitor and has been used extensively in preclinical research (Tang et al., 2019; Zheng et al., 2020). Liproxstatin-1 has been shown to suppress ferroptosis by subverting the lipid-peroxidation process, and its anti-ferroptosis effect is considered superior to that of other lipid-autoxidation inhibitors (e.g., ferrostatin-1) (Zilka et al., 2017). Because we previously demonstrated the potential role of lipid peroxidation in spinal ferroptosis under chronic pain conditions (Guo et al., 2021), we selected this compound as the ferroptosis inhibitor in this study. For 3 consecutive days after CFA injection, 30 μL liproxstatin-1 (10 μg/μL, abs810754, Absin Bioscience Inc., Shanghai, China) or the same amount of vehicle (dimethyl sulfoxide, 10 μg/μL) was injected into the CFA-Lip or CFA-Veh rats via the intrathecal route. The CFA and Con groups did not receive any drug (**Figure 1A**). The above volume of liproxstatin-1 was selected because we observed in our pilot study that a higher volume of 40 μL liproxstatin-1 caused temporary lower limb paralysis (recovery occurred gradually within 3 days of the injection) in two of six rats, whereas there were no significant improvements in mechanical and thermal hypersensitivities when a dose of 20 μL was used (**Additional Tables 1** and **2**). Furthermore, we compared the anti-hyperalgesic effect of liproxstatin-1 with that of minocycline (positive-control pharmacotherapy), the latter of which has been shown to exert a promising therapeutic effect in a CFA-induced inflammatory-pain rodent model (Zhou et al., 2015; Li et al., 2022). According to previously reported methods (Zhou et al., 2015; Li et al., 2022), minocycline hydrochloride (100 μg; M9511, MilliporeSigma) was dissolved in 30 μL of 0.9% saline and administered daily for 7 successive days via the intrathecal route to the CFA-Mino group.

Behavioral tests

To estimate painful behavior in rats, we performed pain-related behavioral tests based on tactile stimulus methods. Baseline values were measured 3 days before CFA administration. On the first, third, fifth, and seventh days after CFA injection, an independent investigator, who had no knowledge of the group allocation, measured the mechanical and thermal sensitivities of all five rats in the CFA-Mino group and five random rats in each of the remaining four groups before intrathecal drug administration (**Figure 1A**). To allow acclimation to the testing environment and apparatus, each animal was separately placed into the testing boxes at least 30 minutes before the tests. In each rat, thermal sensitivity measurements were obtained 30 minutes after obtaining the mechanical sensitivity measurements.

As described earlier (Guo et al., 2021), mechanical sensitivity was assessed by perpendicularly pushing multiple calibrated von Frey fibers (North Coast Medical, Morgan Hill, CA, USA) against the mid-plantar surface of the hind paw to increase stiffness (1.0, 1.4, 2.0, 4.0, 6.0, 8.0, 10.0, 15.0, and 26.0 g), and a positive sign was represented by a paw withdrawal in response to the tactile stimuli a minimum of three out of five testing performances. The lowest bending force that generated a positive response was considered the paw mechanical withdrawal threshold (PMWT).

Thermal sensitivity was quantified using radiant heat equipment (UGO BASILE Plantar Test Apparatus, Varese, Italy), which was placed under the rat's hind paw. Based on our previous study (Guo et al., 2021), the maximum heating time was set to 25 seconds because a longer cutoff latency increases the risk of burns on the rat's hind paw tissue. The thermal hyperalgesia test was repeated a minimum of five times at 10-minute intervals, and the paw thermal withdrawal latency (PTWL) was calculated as the mean latency of the withdrawal response, which was characterized by a lift or lick of the hind paw, across five tests.

Iron content and lipid peroxidation assays

On the seventh day after CFA or saline administration, the ipsilateral (CFA injection side) spinal cord enlargement and DRG tissues at L4–L6 were collected from three random rats per group. In line with previous studies (Ozen et al., 2011; Guo et al., 2021), iron content was measured using flame atomic absorption spectrophotometry, expressed as micrograms per gram sample, and estimated by contrasting with the absorbance to a series of standard concentrations of ferrous sulfate (FeSO4). Commercial assay kits were used to estimate the levels of malondialdehyde (MDA, Jiancheng Biology, Nanjing, Jiangsu, China, A003-1), superoxide dismutase (SOD, Jiancheng Biology, A001-1), and glutathione peroxidase (GSH-Px, Jiancheng Biology, A005-1) in line with the manufacturer's handbook. ROS generation was determined using 2,7-dichlorodihydrofluorescein diacetate (Thermo Fisher Scientific, Waltham, MA, USA) in accordance with a previous publication (Chung et al., 2015).

Western blot analysis

The ipsilateral (CFA injection side) spinal cord enlargement and DRG tissues at L4–L6 of three random rats per group were collected 1 week after CFA or saline administration and homogenized in a lysis buffer that consisted of RIPA (radio immunoprecipitation assay) and protease inhibitor phenylmethanesulfonylfluoride (50:1, Beyotime Institute of Biotechnology, Shanghai, China). The western blotting analysis protocols were conducted in line with those reported previously (Cheng et al., 2019). Briefly, the total protein was extracted from the collected spinal cord and DRG tissues using RIPA lysis buffer (Solarbio, Beijing, China), and the protein concentration was evaluated using a BCA (bicinchoninic acid) protein assay kit (Bio-Rad, Hercules, CA, USA). Equal amounts of protein were separated in a 10% sodium dodecyl sulfate-polyacrylamide gel electrophoresis gel (Solarbio) and transferred to a nitrocellulose membrane after electrophoresis (Merck Millipore, Carrigtwohill, Co. Cork, Ireland). The membrane was blocked for 1 hour with 5% skim milk (Biofroxx, Einhausen, Germany) in TBST (tris buffered saline with tween 20) at room temperature and subsequently incubated with a primary antibody overnight at 4°C. The following primary antibodies were applied: rabbit polyclonal antibody to ACSL4 (1:1000 for the spinal cord and DRG; ABclonal, Wuhan, Hubei, China, Cat# A6826; RRID: AB_2767400), rabbit monoclonal antibody to GPX4 (1:1000 for the spinal cord and DRG; Abcam, Cambridge, UK, Cat# ab125066; RRID: AB_10973901), and rabbit monoclonal antibody to beta-actin (β-actin) (1:100,000 for the spinal cord and DRG; ABclonal, Cat# AC026; RRID: AB_2768234). Images were acquired using a Tanon 5500 chemiluminescent imaging system (Tanon, Shanghai, China), and the intensities of the protein bands were quantitatively determined by densitometry using ImagePro Plus (version 6.0, National Institutes of Health, Bethesda, MD, USA) and normalized according to the β-actin band intensities.

Immunofluorescence

The immunofluorescence analysis protocols were conducted in line with those of our previous study (Guo et al., 2021). After transcardial perfusion with 0.1 M phosphate-buffered saline (PBS), followed by 4% paraformaldehyde, the

ipsilateral (CFA injection side) L4–L6 spinal cord enlargement and DRG tissues of three random rats per group were collected and sectioned into 10-μm-thick specimens on a freezing microtome (MICROM, Walldorf, Germany, HM550VP). To determine the specific cellular distribution of the ferroptosis marker ACSL4 in the spinal cord and DRG tissues, we performed double staining using a rabbit polyclonal antibody to ACSL4 (1:200 for the spinal cord and 1:500 for the DRG, ABclonal, Cat# A6826, RRID: AB_2767400) and one of the following cell markers: neuronal nucleus (NeuN) as a specific neuronal marker (mouse monoclonal antibody, 1:200 for the spinal cord and 1:500 for the DRG, Abcam, Cat# ab104224, RRID: AB_10711040), glial fibrillary acidic protein (GFAP) as a hallmark of astrocyte or satellite glial cell (mouse monoclonal antibody, 1:200 for the spinal cord and 1:500 for the DRG, Abcam, Cat# ab10062, RRID: AB_296804), ionized calcium-binding adapter molecule 1 (Iba-1) as a hallmark of microglia (mouse monoclonal antibody, 1:200 for the spinal cord, Abcam, Cat# ab15690, RRID: AB_2224403), 2′3′-cyclic nucleotide 3′-phosphodiesterase (CNPase) as a hallmark of mature oligodendrocytes (mouse monoclonal antibody, 1:100 for the spinal cord, Abcam, Cat# ab6319, RRID: AB_2082593), and S100 calcium binding protein B (S100β) as a hallmark of Schwann cells (mouse monoclonal antibody, 1:200 for the DRG, Immunoway Biotechnology, Plano, TX, USA, Cat# YM0572) at 4°C overnight in a humid box. After three 5-minute washes with PBS, the slices were incubated with the following secondary antibodies: Alexa 594-labeled goat anti-mouse immunoglobulin G (IgG, 1:500, Abcam, Cat# ab150120, RRID: AB_2631447) or Alexa 488-labeled goat anti-rabbit IgG (1:500, Abcam, Cat# ab150081, RRID: AB_2734747) for 1 hour at room temperature. Sections were observed under a Thermo Fisher EVOS FL Auto laser confocal scanning microscope (Thermo Fisher Scientific Inc.). Five fields per rat were randomly selected for performing quantitative analysis using ImageJ (version 1.8.0, National Institutes of Health, Bethesda, MD, USA). As previously described (Batista et al., 2019; Zhang et al., 2022), the average fluorescence intensity of each pixel was normalized to the background intensity of the same image, and the ratio of overlapped pixels ($ACSL4^+$/cell marker$^+$) from the total cell marker+ pixels was used to measure the degree of colocalization in the spinal cord and DRG tissues.

Transmission electron microscope

On the seventh day following CFA/saline administration, three random rats per group were sacrificed and perfused with a mixed agent (2% paraformaldehyde and 2% glutaraldehyde in 0.1 M sodium cacodylate). Sequentially, the ipsilateral (CFA injection side) spinal cord enlargement and DRG tissues at L4–L6 were collected and post-fixed in 2% osmium tetroxide with 1.6% potassium ferrocyanide in 0.1 M sodium cacodylate. This was followed by sample cutting and dehydration with a graded ethanol (50%, 70%, and 90%) and acetone (100%) series. After embedding in Eponate 812 medium (90529–77–4, Structure Probe, Inc., West Chester, PA, USA), the sections were transferred to copper mesh grids and stained with 2% uranyl acetate and lead citrate. The ultrastructure of mitochondria was visualized in different types of spinal cord (neurons, astrocytes, microglia, and oligodendrocytes) and DRG-tissue (neurons, satellite glial cells, and Schwann cells) cells using transmission electron microscopy (Hitachi, Ltd., HT-7700, Hitachi, Tokyo, Japan). The ratio of mitochondria with aberrant architectural changes (e.g., rupture of cristae and membranes) to total mitochondria was calculated and averaged across five random fields per rat.

Statistical analysis

Sample size was not predetermined using any statistical methods; however, our sample sizes were similar to those reported in a previous publication (Guo et al., 2021). We performed statistical comparisons using SPSS 20.0 statistical software (IBM Corp., Armonk, NY, USA). All values are expressed as means ± standard deviations (SDs). For the comparisons of PMWT and PTWL values, we used a two-way repeated-measures analysis of variance (ANOVA) followed by Bonferroni *post hoc* tests. A one-way analysis of variance followed by Bonferroni *post hoc* tests was used to compare other data among groups. In all cases, statistical significance was set at $P < 0.05$.

Results

Intrathecal liproxstatin-1 administration reduces CFA-induced painful behaviors

Baseline PMWT and PTWL values recorded before CFA/saline injection into the hind paw did not differ significantly among the groups of rats receiving different treatments (PMWT: $P = 0.320$, PTWL: $P = 0.685$). Compared with saline treatment, a single CFA injection induced hypersensitive behaviors in response to mechanical and thermal stimuli in rats during the entire experimental period ($P_{Con\ vs.\ CFA} < 0.001$ after CFA/saline injection; **Figure 1B** and **C**), which indicated that the chronic inflammatory-pain model was successfully constructed. After intrathecal administration of the potent ferroptosis inhibitor liproxstatin-1 for 3 consecutive days following CFA injection, the PMWT and PTWL of CFA-treated rats were dramatically elevated in comparison with those of the CFA-Veh rats (PMWT: $P_{CFA\text{-}Lip\ vs.\ CFA\text{-}Veh} < 0.01$ on the third and fifth days and $P_{CFA\text{-}Lip\ vs.\ CFA\text{-}Veh} < 0.001$ on the seventh day after CFA injection; PTWL: $P_{CFA\text{-}Lip\ vs.\ CFA\text{-}Veh} < 0.01$ on the third and fifth days and $P_{CFA\text{-}Lip\ vs.\ CFA\text{-}Veh} < 0.001$ on the seventh day after CFA injection; **Figure 1B** and **C**). Moreover, there were no significant differences in PMWT or PTWL between the liproxstatin-1- and minocycline-treated groups during the study period (**Figure 1B** and **C**).

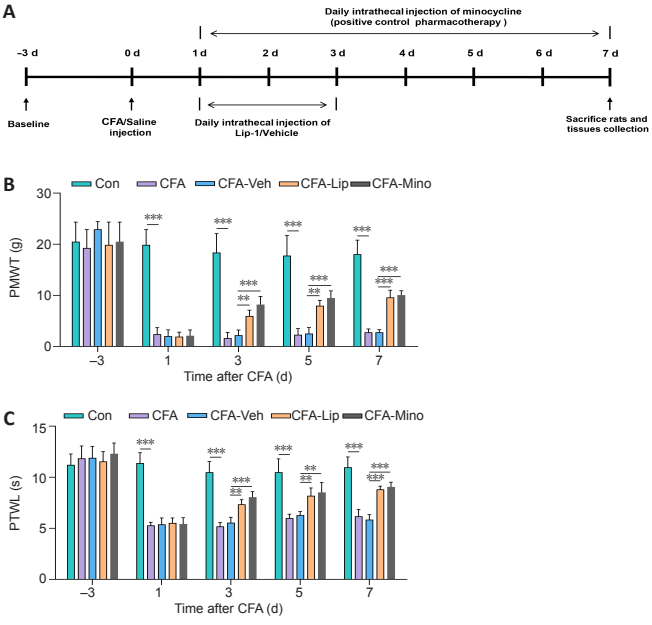

Figure 1 | Attenuation of mechanical and thermal hypersensitivities following intrathecal liproxstatin-1 administration.

(A) A diagram showing the experimental timeline. Baseline thresholds were obtained 3 days before complete Freund's adjuvant (CFA) injection. On day 0, rats received 100 μL of CFA or saline as vehicle control to establish the inflammatory pain model. (B) PMWT and (C) PTWL values were reduced following CFA treatment, and intrathecal liproxstatin-1 or minocycline administration attenuated these mechanical and thermal hypersensitivities in CFA-treated rats. Data in bar charts are expressed as the mean ± SD and represent the results of three independent experiments in five rats per group. Data were analyzed using two-way repeated-measures analysis of variance followed by Bonferroni *post hoc* tests. $^{**}P < 0.01$, $^{***}P < 0.001$. Lip: Liproxstatin-1; Mino: minocycline; PMWT: paw mechanical withdrawal threshold; PTWL: paw thermal withdrawal latency; Veh: vehicle

Liproxstatin-1 reduces levels of iron content and lipid peroxidation hallmarks in the spinal cord and DRG of rats treated with CFA

Iron overload and stimulation of lipid peroxisome proliferation are considered key regulators of ferroptosis (Guo et al., 2021). Thus, we subsequently determined the levels of iron content and several core factors of redox homeostasis in the spinal cord and DRG tissues. CFA treatment via the hind paw significantly enhanced iron levels in the rat spinal cord ($P_{Con\ vs.\ CFA} < 0.001$; **Figure 2A**) and DRG tissues ($P_{Con\ vs.\ CFA} < 0.001$; **Figure 2B**) compared with those in the Con group. Iron overload was significantly alleviated in the spinal cord ($P_{CFA\text{-}Lip\ vs.\ CFA\text{-}Veh} < 0.001$; **Figure 2A**) and DRG tissues ($P_{CFA\text{-}Lip\ vs.\ CFA\text{-}Veh} = 0.047$; **Figure 2B**) in CFA rats after intrathecal administration of ferroptosis inhibitor liproxstatin-1.

In addition to iron accumulation, injection of CFA induced lipid peroxidation, as reflected by significant rises in ROS fold changes (spinal cord: $P_{Con\ vs.\ CFA} < 0.001$; **Figure 2C**; DRG: $P_{Con\ vs.\ CFA} < 0.001$; **Figure 2D**) and MDA concentrations (spinal cord: $P_{Con\ vs.\ CFA} < 0.001$; **Figure 2E**; DRG: $P_{Con\ vs.\ CFA} < 0.001$; **Figure 2F**) and decreases in SOD (spinal cord: $P_{Con\ vs.\ CFA} = 0.002$, **Figure 2G**; DRG: $P_{Con\ vs.\ CFA} < 0.001$; **Figure 2H**) and GSH-Px levels (spinal cord: $P_{Con\ vs.\ CFA} < 0.001$; **Figure 2I**; DRG: $P_{Con\ vs.\ CFA} = 0.004$; **Figure 2J**) in both the spinal cord and DRG tissues. Intrathecal delivery of liproxstatin-1 to CFA rats significantly lowered the rise in ROS (spinal cord: $P_{CFA\text{-}Lip\ vs.\ CFA\text{-}Veh} < 0.001$; **Figure 2C**; DRG: $P_{CFA\text{-}Lip\ vs.\ CFA\text{-}Veh} = 0.001$; **Figure 2D**) and MDA levels (spinal cord: $P_{CFA\text{-}Lip\ vs.\ CFA\text{-}Veh} = 0.020$; **Figure 2E**; DRG: $P_{CFA\text{-}Lip\ vs.\ CFA\text{-}Veh} = 0.019$; **Figure 2F**) but activated the decrease in SOD (spinal cord: $P_{CFA\text{-}Lip\ vs.\ CFA\text{-}Veh} = 0.001$; **Figure 2G**; DRG: $P_{CFA\text{-}Lip\ vs.\ CFA\text{-}Veh} = 0.008$; **Figure 2H**) and GSH-Px levels (spinal cord: $P_{CFA\text{-}Lip\ vs.\ CFA\text{-}Veh} = 0.012$; **Figure 2I**; DRG: $P_{CFA\text{-}Lip\ vs.\ CFA\text{-}Veh} = 0.042$, **Figure 2J**) in the spinal cord and DRG tissues.

Liproxstatin-1 treatment diminishes ACSL4 protein levels and increases GPX4 protein levels

Various proteins, such as ACSL4 and GPX4, are considered crucial ferroptosis-regulating factors. Therefore, we focused on the levels of ACSL4 and GPX4 in the spinal cord and DRG tissues. CFA treatment significantly upregulated ACSL4 levels and downregulated GPX4 levels in the spinal cord (ACSL4: $P_{Con\ vs.\ CFA} < 0.001$; GPX4: $P_{Con\ vs.\ CFA} = 0.026$; **Figure 3A–C**) and DRG tissues (ACSL4: $P_{Con\ vs.\ CFA} = 0.001$; GPX4: $P_{Con\ vs.\ CFA} = 0.002$, **Figure 3D–F**). Intrathecal liproxstatin-1 delivery restored ACSL4 and GPX4 expression disorders secondary to CFA injection in both the spinal cord (ACSL4: $P_{CFA\text{-}Lip\ vs.\ CFA\text{-}Veh} = 0.003$; GPX4: $P_{CFA\text{-}Lip\ vs.\ CFA\text{-}Veh} = 0.002$; **Figure 3A–C**) and DRG tissues (ACSL4: $P_{CFA\text{-}Lip\ vs.\ CFA\text{-}Veh} = 0.002$; GPX4: $P_{CFA\text{-}Lip\ vs.\ CFA\text{-}Veh} = 0.019$; **Figure 3D–F**).

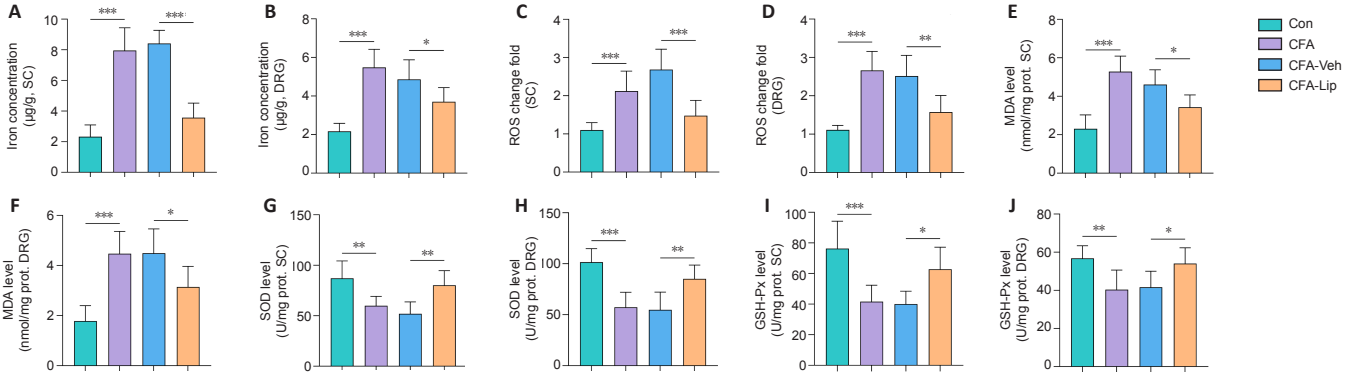

Figure 2 | **Restoration of CFA-induced iron overload and lipid peroxidation, which contributed to pain-like behaviors following intrathecal liproxstatin-1 administration.**
Levels of iron content and lipid peroxidation hallmarks in the spinal cord (SC) and DRG tissues. Intrathecal liproxstatin-1 administration decreased iron, reactive oxygen species (ROS), and malondialdehyde (MDA) levels and increased superoxide dismutase (SOD) and glutathione peroxidase (GSH-Px) levels in the spinal cord and DRG of CFA rats. Data are expressed as the mean ± SD and represent the results of three independent experiments in three rats per group. Data were analyzed using one-way analysis of variance followed by Bonferroni *post hoc* tests. *P < 0.05, **P < 0.01, ***P < 0.001. CFA: Complete Freund's adjuvant; DRG: dorsal root ganglion; GSH-Px: glutathione peroxidase; Lip: liproxstatin-1; MDA: malondialdehyde; Mino: minocycline; prot: protein; ROS: reactive-oxygen-species; SOD: superoxide dismutase; Veh: vehicle.

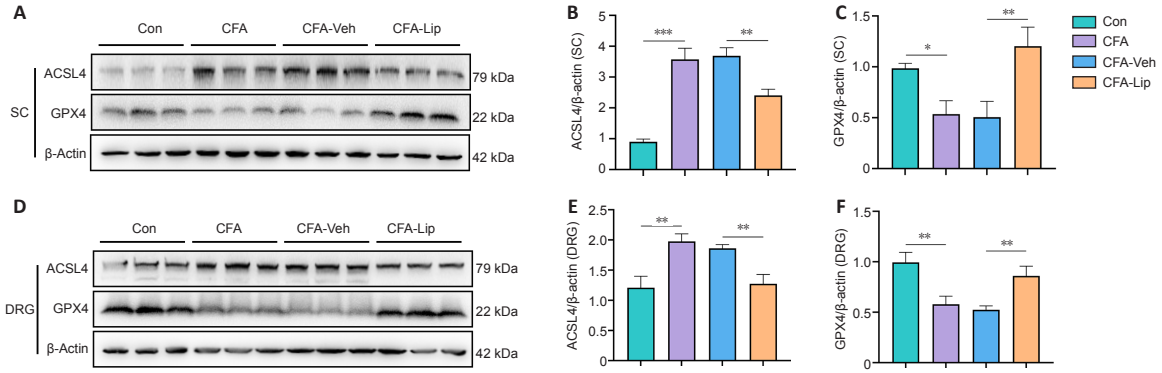

Figure 3 | **Anti-acyl-CoA synthetase long-chain family member 4 (ACSL4) decreases and glutathione peroxidase 4 (GPX4) increases in CFA rats following intrathecal liproxstatin-1 administration**
(A–C) The representative bands and quantitative evaluations of ACSL4 and GPX4 protein levels demonstrated that liproxstatin-1 restored the abnormal levels of ACSL4 and GPX4 in the spinal cord (SC) of CFA rats. (D–F) The representative bands and quantitative evaluations of ACSL4 and GPX4 protein levels demonstrated that liproxstatin-1 restored the abnormal levels of ACSL4 and GPX4 in the dorsal root ganglion tissue of CFA rats. Data in bar charts are expressed as the mean ± SD and represent results of three independent experiments in three rats per group. Data were analyzed using one-way analysis of variance followed by Bonferroni *post hoc* tests. *P < 0.05, **P < 0.01, ***P < 0.001. ACSL4: Anti-acyl-coenzyme A synthetase long-chain family member 4; CFA: complete Freund's adjuvant; GPX4: glutathione peroxidase 4; Lip: liproxstatin-1; Mino: minocycline; Veh: vehicle.

Cellular localization of ACSL4 in the spinal dorsal horn and DRG

Using the double-immunofluorescence staining method, we investigated the ACSL4 protein distribution in defined cellular compartments in the rat spinal cord and DRG tissues. After CFA injection, ACSL4 colocalized primarily with the microglial marker Iba-1 ($P_{CFA\ vs.\ Con}$ = 0.008), the astrocyte marker GFAP ($P_{CFA\ vs.\ Con}$ < 0.001), and oligodendrocyte marker CNPase ($P_{CFA\ vs.\ Con}$ < 0.001) in the spinal tissues (**Figure 4**). In addition, CFA administration enhanced the expression of ACSL4 in the satellite glial cells labeled by GFAP ($P_{CFA\ vs.\ Con}$ = 0.002) and Schwann cells labeled by S100β ($P_{CFA\ vs.\ Con}$ < 0.001) in DRG tissues (**Figure 5**). These results suggested that the injection of CFA into the hind paw predominantly causes the widespread presence of ferroptosis in glial and Schwann cells in the rat spinal cord and DRG tissues. Notably, intrathecal liproxstatin-1 delivery led to a significant reduction in ACSL4 immunoreactivity in astrocytes ($P_{CFA\text{-}Lip\ vs.\ CFA\text{-}Veh}$ = 0.001), microglia ($P_{CFA\text{-}Lip\ vs.\ CFA\text{-}Veh}$ = 0.002), and oligodendrocytes ($P_{CFA\text{-}Lip\ vs.\ CFA\text{-}Veh}$ = 0.013) in the spinal cord (**Figure 4**), as well as satellite glial ($P_{CFA\text{-}Lip\ vs.\ CFA\text{-}Veh}$ = 0.018) and Schwann cells ($P_{CFA\text{-}Lip\ vs.\ CFA\text{-}Veh}$ = 0.001) in the DRG (**Figure 5**).

Liproxstatin-1 suppresses CFA-induced abnormal morphological changes in the mitochondria in the spinal cord and DRG

One of the classical pathological changes during ferroptosis is the abnormal morphological characteristics of the mitochondria (Dixon et al., 2012). In response to CFA injection, the mitochondria showed unusual morphological features, such as cristae rupture and greater membrane density in the spinal cord (**Figure 6**) and DRG tissues (**Figure 7**). Interestingly, although representative ferroptosis-like changes in the mitochondria were observed in the spinal and DRG neurons, quantitative analysis revealed higher ratios of mitochondria that represented morphological disorders in response to CFA administration in the non-neural cells of the spinal cord ($P_{CFA\ vs.\ Con}$ < 0.001 for astrocytes, microglia, and oligodendrocytes; **Figure 6**) and DRG ($P_{CFA\ vs.\ Con}$ < 0.001 for satellite glial and Schwann cells; **Figure 7**). Moreover, intrathecal injection of liproxstatin-1 into CFA rats not only reversed the abnormal mitochondrial changes but also resulted in a significant reduction in the abnormal mitochondria ratio in the non-neural spinal cord ($P_{CFA\text{-}Lip\ vs.\ CFA\text{-}Veh}$ < 0.001 for astrocytes, $P_{CFA\text{-}Lip\ vs.\ CFA\text{-}Veh}$ = 0.003 for microglia, and $P_{CFA\text{-}Lip\ vs.\ CFA\text{-}Veh}$ < 0.001 for oligodendrocytes; **Figure 6**) and DRG cells ($P_{CFA\text{-}Lip\ vs.\ CFA\text{-}Veh}$ < 0.001 for satellite cells and $P_{CFA\text{-}Lip\ vs.\ CFA\text{-}Veh}$ = 0.023 for Schwann cells; **Figure 7**).

Discussion

As a response to inflammatory factors, inflammatory pain is considered a global clinical problem that diminishes the quality of life of patients (Conaghan et al., 2019). Several studies have revealed that the inflammatory response and ferroptosis share several common features, such as iron accumulation and lipid peroxidation (Singh and Vinayak, 2015; Sun et al., 2021). However, the role of oxidative and iron-driven ferroptosis from an inflammatory pain perspective remains unclear. The current study is the first to identify ferroptosis-like cell death in the spinal cord and DRG in an inflammatory-pain rodent model. Moreover, although previous studies have demonstrated the effects of liproxstatin-1 and ferrostatin-1 (delivered intraperitoneally at a dose of 10 mg/kg in a neuropathic-pain model) (Guo et al., 2021; Wang et al., 2021), whether the administration of ferroptosis inhibitors via the intrathecal route induces an effective analgesic effect against inflammatory pain remains inconclusive. In this study, we found that injection of liproxstatin-1 into the spinal intrathecal space at a relatively low dose (10 μg/μL and 30 μL) effectively hinders spinal ferroptosis and alleviates CFA-induced mechanical allodynia and thermal hyperalgesia. Compared with other drug administration routes, intrathecal drug delivery is particularly advantageous for precisely delivering drugs into the spinal intrathecal space, without the need to consider the permeability of the blood-brain barrier or toxicity to other organs (Cui et al., 2015; Hou et al., 2016). Thus, our results offer a reasonable method to clinically alleviate inflammatory pain. Remarkably, intrathecal injection of 40 μL liproxstatin-1 caused temporary lower limb paralysis in some rats, which suggested that the adverse effects of intrathecal liproxstatin-1 injection were dose-related. Therefore, additional preclinical investigations that clarify the prospects of intrathecal liproxstatin-1 administration for the treatment of inflammatory pain are warranted.

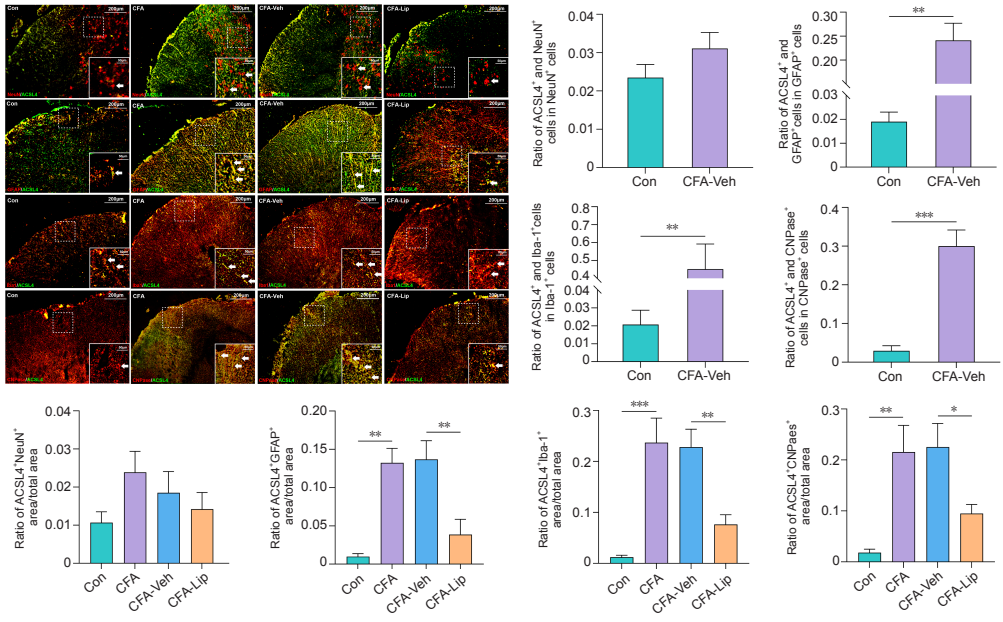

Figure 4 | **Distribution of anti-acyl-coenzyme A synthetase long-chain family member 4 (ACSL4) in distinct cell types in the spinal cord.**
Representative double-immunofluorescence staining images show the distribution of ACSL4 in the spinal cord tissue. The white arrows indicate spinal cells stained with distinct cell markers. Scale bar: 200 μm (50 μm in the magnified boxes). Quantification analyses of cells colocalized by ACSL4 revealed that CFA injection into the hind paw caused widespread ferroptosis in spinal astrocytes, microglia, and oligodendrocytes. Intrathecal treatment of liproxstatin-1 dramatically decreased the ratio of ACSL4 immunoreactivity area to astrocyte/microglia/oligodendrocyte marker immunoreactivity area in spinal cord. Data in bar charts are expressed as the mean ± SD and represent results of five sections per rat with three rats per group. Data were analyzed using one-way analysis of variance, followed by Bonferroni *post hoc* tests. **P* < 0.05, ***P* < 0.01, ****P* < 0.001. ACSL4: Anti-acyl-coenzyme A synthetase long-chain family member 4; CFA: complete Freund's adjuvant; Lip: liproxstatin-1; Mino: minocycline; Veh: vehicle.

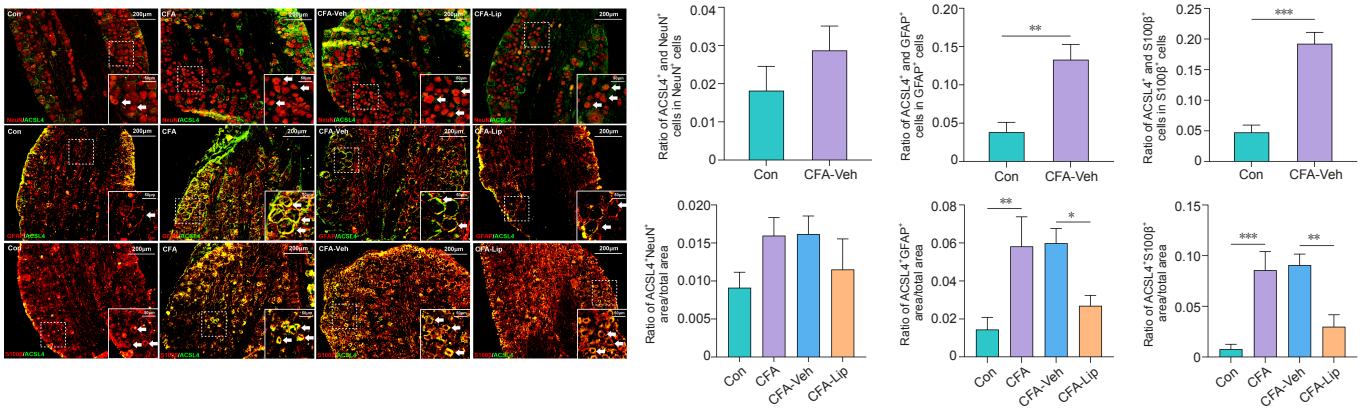

Figure 5 | **Distribution of anti-acyl-coenzyme A synthetase long-chain family member 4 (ACSL4) in distinct cell types in the dorsal root ganglion (DRG) cells.**
Representative double-immunofluorescence staining images show the distribution of the ACSL4 protein in the DRG tissues. The white arrows indicate DRG cells stained with distinct cell markers. Scale bar: 200 μm (50 μm in the magnified boxes). Quantification analyses of cells colocalized by ACSL4 revealed that CFA injection into the hind paw caused widespread ferroptosis in the satellite glial and Schwann cells of the rat DRG. Intrathecal treatment of liproxstatin-1 dramatically decreased the ratio of ACSL4 immunoreactivity to satellite glial cell/Schwann cell marker immunoreactivity area in DRG. Data in bar charts are expressed as the mean ± SD and represent results from five sections per rat with three rats per group. Data were analyzed using one-way analysis of variance followed by Bonferroni *post hoc* tests. **P* < 0.05, ***P* < 0.01, ****P* < 0.001. ACSL4: Anti-acyl-coenzyme A synthetase long-chain family member 4; CFA: complete Freund's adjuvant; DRG: dorsal root ganglion; Lip: liproxstatin-1; Mino: minocycline; Veh: vehicle.

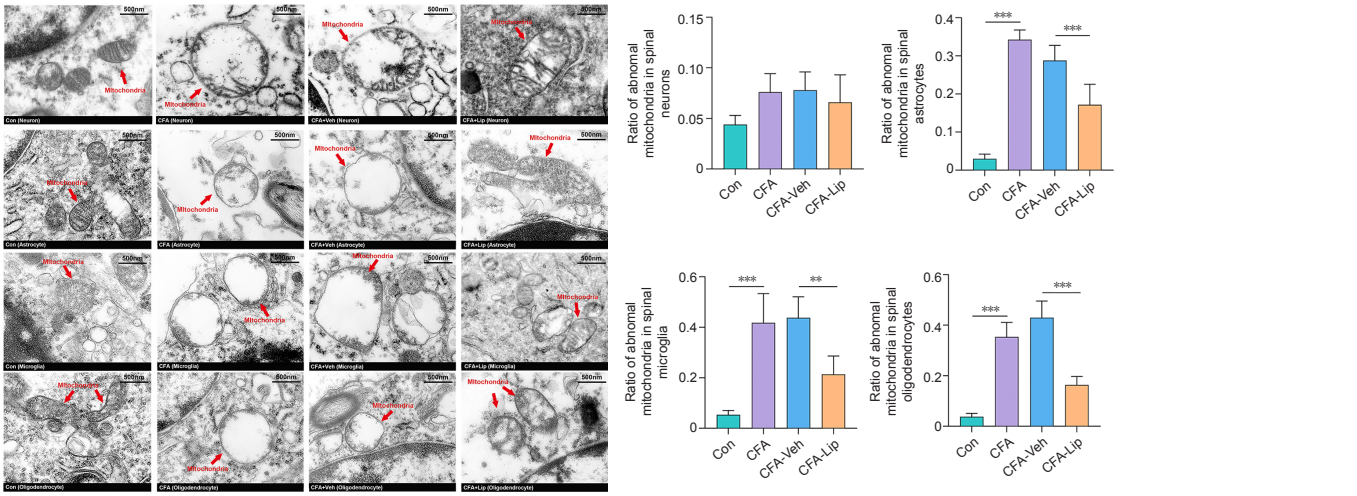

Figure 6 | **Liproxstatin-1-induced protection against mitochondrial morphological changes caused by CFA in the spinal cord.**
Representative electron micrographs of the mitochondrial ultrastructure (red arrows) in the spinal cord across four groups. Scale bar: 500 nm. Quantification analyses showed that intrathecal liproxstatin-1 administration to CFA rats significantly reduced the ratios of abnormal mitochondria to the total mitochondria in spinal astrocytes, microglia, and oligodendrocytes. Data in bar charts are expressed as the mean ± SD and represent results of five sections per rat with three rats per group. Data were analyzed using one-way analysis of variance followed by Bonferroni *post hoc* tests. ***P* < 0.01, ****P* < 0.001. CFA: Complete Freund's adjuvant; Lip: liproxstatin-1; Mino: minocycline; Veh: vehicle.

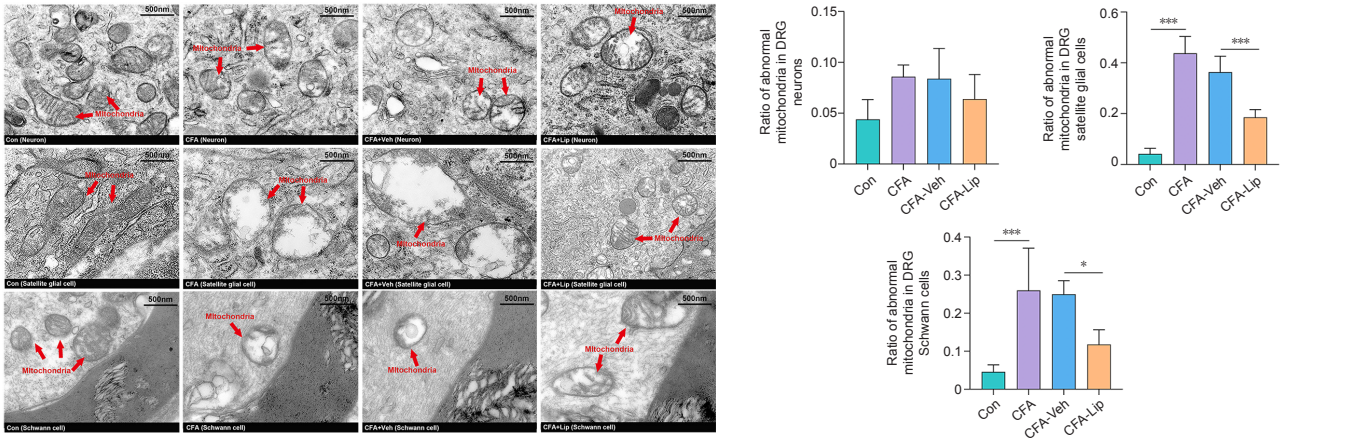

Figure 7 | **Liproxstatin-1-induced protection against mitochondrial morphological changes caused by CFA in dorsal root ganglion (DRG) cells.**
Representative electron micrographs of the mitochondrial ultrastructure (red arrows) in the DRG across four groups. Scale bar: 500 nm. Quantification analyses showed that intrathecal liproxstatin-1 administration to CFA rats significantly reduced the ratios of abnormal mitochondria to the total mitochondria in DRG satellite glial and Schwann cells. Data in bar charts are expressed as the mean ± SD and represent results of five sections per rat with three rats per group. Data were analyzed using one-way analysis of variance followed by Bonferroni *post hoc* tests. *$P < 0.05$, ***$P < 0.001$. CFA: Complete Freund's adjuvant; DRG: dorsal root ganglion; Lip: liproxstatin-1; Mino: minocycline; Veh: vehicle.

It has been shown that DRG tissues transmit nociceptive stimuli to the spinal cord and brain in the form of electrical action potentials (Cui et al., 2021; Ma et al., 2021; Guo et al., 2022). Compelling evidence has indicated that the differential occurrence of multiple pain-related pathophysiological changes in the spinal cord and DRG acts as a trigger during the pathological process of nociceptive hypersensitivity of chronic inflammatory pain (Garcia et al., 2021; Li et al., 2021). For example, changes in programmed cell death, such as autophagy (Chen and Lu, 2017; Yin et al., 2018) and apoptosis (Kahya et al., 2017; Dai et al., 2020), are consistent across both spinal cord and DRG tissues under chronic pain conditions. Moreover, researchers have verified the mechanisms of spinal ferroptosis under neuropathic pain conditions (Guo et al., 2021; Wang et al., 2021); however, implications for ferroptosis in the DRG after painful injuries remain unclear. Our results suggest that ferroptosis-like cell death is enhanced simultaneously in the DRG and spinal cord of CFA rats and is characterized by mitochondrial morphological abnormalities, overwhelming accumulation of iron and lipid peroxisome proliferation, and disorders of expression levels of several ferroptosis biomarkers (i.e., ACSL4 and GPX4). In addition, our data showed that intrathecal injections of liproxstatin-1 successfully alleviated CFA-induced pain-like behaviors, partly via inhibition of the ferroptosis process in the spinal cord and DRG. Taken together, we conclude that ferroptosis plays a crucial role in the CFA-induced sensitization of both DRG and spinal cord tissues.

Although the exact mechanism underlying ferroptosis remains elusive, iron overload has been identified as the most likely trigger of cell death (Dixon et al., 2012). Given its role as a predominant trace element, iron is essential for maintaining cell functions and mediates various important physiological processes, which include but are not limited to hemoglobin synthesis, oxygen transport, and adenosine triphosphate production (Koleini et al., 2021). Iron overload may generate excessive ROS production via Fenton or Haber Weiss reactions, which can induce oxidative stress injury to DNA and proteins and even ferroptosis-like cell death (Alves et al., 2021). Moreover, emerging evidence has established a link between iron homeostasis and the occurrence of inflammatory pain (Sun et al., 2021). For instance, the release of pro-inflammatory cytokine in the cavum articulare was reported to result from the deposit of hemosiderin, an intracellular iron complex that is closely associated with joint pain (Heiland et al., 2010; van Vulpen et al., 2015; Sun et al., 2021). Accordingly, the current study revealed significant iron accumulation in the spinal cord and DRG tissues in CFA rats that exhibited painful behaviors, which suggested that iron overload contributes to ferroptosis activation during CFA-induced inflammatory pain.

Another contributory mechanism of ferroptosis is lipid peroxidation (Lee et al., 2021). At the molecular level, the contributions of GPX4 and ACSL4 to lipid peroxidation injury during ferroptosis have been demonstrated recently (Doll et al., 2017; Tang et al., 2019; Zhang et al., 2021b). When cells are treated with a ferroptosis inducer, the reduced expression of GPX4 and enhanced expression of ACSL4 that respond to an excessive iron level may suppress GSH activity and increase polyunsaturated fatty acyl phospholipids, phospholipids, and oxidized phosphatidylethanolamine levels, which would eventually elicit membrane lipid peroxidation and oxidative stress damage (Doll et al., 2017; Zhang et al., 2021b). Our current work showed that injection of CFA negatively regulates GPX4 level and positively regulates ACSL4 level in the spinal cord and DRG tissues. Consistent with a previous study (Singh and Vinayak, 2015), we also found disordered levels of several lipid peroxidation hallmarks, including the downregulated expression of MDA and GSH-Px levels and the upregulated expression of ROS and MDA levels. Administration of a ferroptosis inhibitor restored GPX4 and ACSL4 levels and alleviated the lipid peroxidation that resulted from CFA treatment. These findings indicated that ferroptosis caused by CFA is involved in GPX4 and ACSL4 dysfunction-induced lipid peroxidation in the context of mechanical allodynia and thermal hyperalgesia.

Our previous study identified ferroptosis-like cell death throughout spinal neurons and glial cells in a neuropathic-pain rodent model (Guo et al., 2021). Interestingly, in the present study, we demonstrated that ferroptosis-related ACSL4 dysregulation and mitochondrial changes were detected primarily in non-neural cells in the spinal cord and DRG under a CFA-induced inflammatory pain condition. Recently, the possible pathogenesis of non-neural ferroptosis in nervous system diseases has gained attention (Wang et al., 2021). For example, a previous study reported the proinflammatory effect of ferroptosis on glial cells: ferroptotic primary astrocytes in mice release excessive amounts of pro-inflammatory factors (e.g., interleukin (IL)-6 and IL-1β), and ferrostatin-1 treatment inhibits inflammatory-factor overproduction (Li et al., 2021). Moreover, inhibiting ferroptosis in Schwann cells via the over-expression of c-Jun may contribute to the recovery of peripheral-nerve function, which highlights the role that ferroptosis plays in nerve-function injury and repair (Gao et al. 2022). Taken together, these findings indicate that non-neural ferroptosis is closely associated with central nervous system inflammation and impairment of peripheral nerve function and that further studies to unmask the exact role of non-neural ferroptosis in CFA-induced inflammatory pain are warranted.

Diminished mitochondrial cristae and increased mitochondrial membrane density usually occur during ferroptosis; moreover, mitochondrial abnormalities have been detected in an inflammatory-pain rodent model (Guo et al., 2013). Our study identified significant disorders of mitochondrial morphological characteristics (e.g., collapsed cristae and disrupted mitochondrial membrane) throughout the non-neural cells in the spinal cord and DRG tissues of CFA-treated rats. Mitochondria have been recognized as a pivotal part of lipid and iron metabolism, and there is a growing interest in understanding the mechanism of mitochondria in ferroptotic cell death (Gan, 2021; Otasevic et al., 2021). Previous studies have identified two enzymes located in mitochondria, citrate synthase and acyl-coenzyme A (CoA) synthetase family member 2, as crucial mediators of erastin-induced ferroptosis owing to their ability to stimulate fatty acid activity and supply precursors during the lipid peroxidation process (Dixon et al., 2012). Moreover, accumulating evidence has suggested that several iron homeostasis-related factors in mitochondria, such as mitoferrin and voltage-dependent anion channels, are functionally relevant to ferroptosis occurrence and that the suppression of two gene-encoding proteins may result in an intracellular accumulation of free iron and promote ferroptosis-like cell death (Shoshan-Barmatz et al., 2010; Otasevic et al., 2021). Our study showed that administration of the ferroptosis suppressor liproxstatin-1 restored the abnormal morphological changes in mitochondria induced by CFA, which suggests that the aberrant mitochondrial morphological characteristics in the spinal cord and DRG tissues are involved in ferroptosis in rats treated with CFA.

This study has several limitations. First, we exclusively focused on the effects of one ferroptosis inhibitor on an inflammatory-pain animal model, and further investigations of other ferroptosis inhibitors are necessary to confirm the role of ferroptosis in inflammatory pain. Second, this preliminary investigation did not completely determine the specific cellular mechanism underlying ferroptosis in the inflammatory-pain process and thus, further investigation is warranted.

Overall, based on an inflammatory-pain animal model with intrathecal CFA injection, our study provided evidence for the occurrence of ferroptosis in the rat spinal cord and DRG tissues, and clarified the effectiveness of intrathecal liproxstatin-1 administration for treating inflammatory pain-like behaviors. These findings highlight the possible link between non-neural ferroptosis and the occurrence of nociceptive responses caused by CFA injection, and demonstrate that this unique form of programmed cell death is a promising therapeutic target for inflammatory pain.

Acknowledgments: *The authors thank Dr. Cui-Cui Xiao from the Third Affiliated Hospital, Sun Yat-sen University for participating in the discussion of the manuscript, and Dr. Jia Chen from the Laboratory Animal Center of South China Agricultural University for assistance in the animal husbandary.*

Author contributions: *Study design: XL; experiment implementation and data acquisition: YFD, JYD; data analysis: PX, JFL; manuscript draft: XL, YFD; manuscript review: XL. All the authors read and approved the final version of manuscript.*

Conflicts of interest: *The authors declare no conflicts of interest.*

Availability of data and materials: *All data generated or analyzed during this study are included in this published article and its supplementary information files.*

Additional files:

Additional Table 1: *Paw withdrawal threshold values (g) of rats that were administered different volumes of liproxstatin-1.*

Additional Table 2: *Paw thermal withdrawal latency (s) of rats that were administered different volumes of liproxstatin-1.*

References

Abbadie C, Brown JL, Mantyh PW, Basbaum AI (1996) Spinal cord substance P receptor immunoreactivity increases in both inflammatory and nerve injury models of persistent pain. Neuroscience 70:201-209.

Alves FM, Kysenius K, Caldow MK, Hardee JP, Crouch PJ, Ayton S, Bush AI, Lynch GS, Koopman R (2021) Iron accumulation in skeletal muscles of old mice is associated with impaired regeneration after ischaemia-reperfusion damage. J Cachexia Sarcopenia Muscle 12:476-492.

Bae C, Wang J, Shim HS, Tang SJ, Chung JM, La JH (2018) Mitochondrial superoxide increases excitatory synaptic strength in spinal dorsal horn neurons of neuropathic mice. Mol Pain 14:1744806918797032.

Baniasadi M, Manaheji H, Maghsoudi N, Danyali S, Zakeri Z, Maghsoudi A, Zaringhalam J (2020) Microglial-induced apoptosis is potentially responsible for hyperalgesia variations during CFA-induced inflammation. Inflammopharmacology 28: 475-485.

Batista CM, Mariano ED, Dale CS, Cristante AF, Britto LR, Otoch JP, Teixeira MJ, Morgalla M, Lepski G (2019) Pain inhibition through transplantation of fetal neuronal progenitors into the injured spinal cord in rats. Neural Regen Res 14: 2011-2019.

Bravo-Hernandez M, Corleto JA, Barragan-Iglesias P, Gonzalez-Ramirez R, Pineda-Farias JB, Felix R, Calcutt NA, Delgado-Lezama R, Marsala M, Granados-Soto V (2016) The alpha5 subunit containing GABAA receptors contribute to chronic pain. Pain 157:613-626.

Chen W, Lu Z (2017) Upregulated TLR3 promotes neuropathic pain by regulating autophagy in rat with L5 spinal nerve ligation model. Neurochem Res 42:634-643.

Cheng N, Zhang Z, Guo Y, Qiu ZL, Du JY, Hei ZQ, Li X (2019) Weighted gene co-expression network analysis reveals specific modules and hub genes related to neuropathic pain in dorsal root ganglions. Biosci Rep 39:BSR20191511.

Chung MK, Asgar J, Lee J, Shim MS, Dumler C, Ro JY (2015) The role of TRPM2 in hydrogen peroxide-induced expression of inflammatory cytokine and chemokine in rat trigeminal ganglia. Neuroscience 297:160-169.

Conaghan PG, Cook AD, Hamilton JA, Tak PP (2019) Therapeutic options for targeting inflammatory osteoarthritis pain. Nat Rev Rheumatol 15:355-363.

Cui W, Yu X, Zhang H (2015) The study of different approaches of parecoxib sodium pretreatment on the behavior of rats with neuropathic pain. Cell Biochem Biophys 72:137-140.

Cui ZK, Li SY, Liao K, Wang ZJ, Guo YL, Tang LS, Tang SB, Ma JH, Chen JS (2021) Characteristics of neural growth and cryopreservation of the dorsal root ganglion using three-dimensional collagen hydrogel culture versus conventional culture. Neural Regen Res 16:1856-1864.

Dai WL, Bao YN, Fan JF, Li SS, Zhao WL, Yu BY, Liu JH (2020) Levo-corydalmine attenuates microglia activation and neuropathic pain by suppressing ASK1-p38 MAPK/NF-kappaB signaling pathways in rat spinal cord. Reg Anesth Pain Med 45:219-229.

Dixon SJ, Lemberg KM, Lamprecht MR, Skouta R, Zaitsev EM, Gleason CE, Patel DN, Bauer AJ, Cantley AM, Yang WS, Morrison B, 3rd, Stockwell BR (2012) Ferroptosis: an iron-dependent form of nonapoptotic cell death. Cell 149:1060-1072.

Doll S, Proneth B, Tyurina YY, Panzilius E, Kobayashi S, Ingold I, Irmler M, Beckers J, Aichler M, Walch A, Prokisch H, Trümbach D, Mao G, Qu F, Bayir H, Füllekrug J, Scheel CH, Wurst W, Schick JA, Kagan VE, et al. (2017) ACSL4 dictates ferroptosis sensitivity by shaping cellular lipid composition. Nat Chem Biol 13:91-98.

Fattori V, Pinho-Ribeiro FA, Staurengo-Ferrari L, Borghi SM, Rossaneis AC, Casagrande R, Verri WA, Jr. (2019) The specialised pro-resolving lipid mediator maresin 1 reduces inflammatory pain with a long-lasting analgesic effect. Br J Pharmacol 176:1728-1744.

Gan B (2021) Mitochondrial regulation of ferroptosis. J Cell Biol 220:e202105043.

Gao D, Huang Y, Sun X, Yang J, Chen J, He J (2022) Overexpression of c-Jun inhibits erastin-induced ferroptosis in Schwann cells and promotes repair of facial nerve function. J Cell Mol Med doi: 10.1111/jcmm.17241.

Garcia G, Martinez-Rojas VA, Murbartian J (2021) TREK-1 potassium channels participate in acute and long-lasting nociceptive hypersensitivity induced by formalin in rats. Behav Brain Res 413:113446.

Guo BL, Sui BD, Wang XY, Wei YY, Huang J, Chen J, Wu SX, Li YQ, Wang YY, Yang YL (2013) Significant changes in mitochondrial distribution in different pain models of mice. Mitochondrion 13:292-297.

Guo TT, Zhao Y, Huang WX, Zhang T, Zhao LL, Gu XS, Zhou SL (2022) Silencing the enhancer of zeste homologue 2, Ezh2, represses axon regeneration of dorsal root ganglion neurons. Neural Regen Res 17:1518-1525.

Guo Y, Du J, Xiao C, Xiang P, Deng Y, Hei Z, Li X (2021) Inhibition of ferroptosis-like cell death attenuates neuropathic pain reactions induced by peripheral nerve injury in rats. Eur J Pain 25:1227-1240.

Heiland GR, Aigner E, Dallos T, Sahinbegovic E, Krenn V, Thaler C, Weiss G, Distler JH, Datz C, Schett G, Zwerina J (2010) Synovial immunopathology in haemochromatosis arthropathy. Ann Rheum Dis 69:1214-1219.

Ho IHT, Liu X, Zou Y, Liu T, Hu W, Chan H, Tian Y, Zhang Y, Li Q, Kou S, Chan CS, Gin T, Cheng CHK, Wong SH, Yu J, Zhang L, Wu WKK, Chan MTV (2019) A novel peptide interfering with proBDNF-Sortilin interaction alleviates chronic inflammatory pain. Theranostics 9:1651-1665.

Hou Y, Wang L, Gao J, Jin X, Ji F, Yang J (2016) A modified procedure for lumbar intrathecal catheterization in rats. Neurol Res 38:725-732.

Huang Y, Chen SR, Chen H, Pan HL (2019) Endogenous transient receptor potential ankyrin 1 and vanilloid 1 activity potentiates glutamatergic input to spinal lamina I neurons in inflammatory pain. J Neurochem 149:381-398.

Jia S, Chen G, Liang Y, Liang X, Meng C (2021) GCH1-regulated miRNAs are potential targets for microglial activation in neuropathic pain. Biosci Rep 41:BSR20210051.

Kahya MC, Naziroglu M, Ovey IS (2017) Modulation of diabetes-induced oxidative stress, apoptosis, and Ca(2+) entry through TRPM2 and TRPV1 channels in dorsal root ganglion and hippocampus of diabetic rats by melatonin and selenium. Mol Neurobiol 54:2345-2360.

Koleini N, Shapiro JS, Geier J, Ardehali H (2021) Ironing out mechanisms of iron homeostasis and disorders of iron deficiency. J Clin Invest 131:e148671.

Lee JY, Kim WK, Bae KH, Lee SC, Lee EW (2021) Lipid metabolism and ferroptosis. Biology (Basel) 10:184.

Li J, Chen Y, Liu J, Zhang D, Liang P, Lu P, Shen J, Miao C, Zuo Y, Zhou C (2021) Elevated expression and activity of sodium leak channel contributes to neuronal sensitization of inflammatory pain in rats. Front Mol Neurosci 14:723395.

Li S, Zhou C, Zhu Y, Chao Z, Sheng Z, Zhang Y, Zhao Y (2021) Ferrostatin-1 alleviates angiotensin II (Ang II)-induced inflammation and ferroptosis in astrocytes. Int Immunopharmacol 90:107179.

Li X, Zhou B, Yang H, Yang X, Zhao Z, Pan Z, Liao X, Jian W, Liu Y, Lu H, Xue Q, Luo Y, Yu B, Huang H, Ma D, Liu Z (2022) Phosphorylation at Ser 727 increases STAT3 interaction with PKCε regulating neuron-glia crosstalk via IL-6-mediated hyperalgesia in vivo and in vitro. Mediators Inflamm 2022:2782080.

Liu B, Luo M, Meng D, Pan H, Shen H, Shen J, Yao M, Xu L (2021) Tetrahydropalmatine exerts analgesic effects by promoting apoptosis and inhibiting the activation of glial cells in rats with inflammatory pain. Mol Pain 17:17448069211042117.

Ma J, Patil V, Pandit A, Quinlan LR, Finn DP, Grad S, Alini M, Peroglio M (2021) In vitro model to investigate communication between dorsal root ganglion and spinal cord glia. Int J Mol Sci 22:9725.

Otasevic V, Vucetic M, Grigorov I, Martinovic V, Stancic A (2021) Ferroptosis in different pathological contexts seen through the eyes of mitochondria. Oxid Med Cell Longev 2021:5537330.

Ozen OA, Kus I, Bakirdere S, Sarsilmaz M, Yaman M (2011) Effects of formaldehyde inhalation on zinc, copper and iron concentrations in liver and kidney of male rats. Biol Trace Elem Res 140:177-185.

Percie du Sert N, Hurst V, Ahluwalia A, Alam S, Avey MT, Baker M, Browne WJ, Clark A, Cuthill IC, Dirnagl U, Emerson M, Garner P, Holgate ST, Howells DW, Karp NA, Lazic SE, Lidster K, MacCallum CJ, Macleod M, Pearl EJ, et al. (2020) The ARRIVE guidelines 2.0: Updated guidelines for reporting animal research. PLoS Biol 18:e3000410.

Shoshan-Barmatz V, De Pinto V, Zweckstetter M, Raviv Z, Keinan N, Arbel N (2010) VDAC, a multi-functional mitochondrial protein regulating cell life and death. Mol Aspects Med 31:227-285.

Singh AK, Vinayak M (2015) Curcumin attenuates CFA induced thermal hyperalgesia by modulation of antioxidant enzymes and down regulation of TNF-alpha, IL-1beta and IL-6. Neurochem Res 40:463-472.

Storkson RV, Kjorsvik A, Tjolsen A, Hole K (1996) Lumbar catheterization of the spinal subarachnoid space in the rat. J Neurosci Methods 65:167-172.

Sun K, Guo Z, Hou L, Xu J, Du T, Xu T, Guo F (2021) Iron homeostasis in arthropathies: From pathogenesis to therapeutic potential. Ageing Res Rev 72:101481.

Tan Q, Fang Y, Gu Q (2021) Mechanisms of modulation of ferroptosis and its role in central nervous system diseases. Front Pharmacol 12:657033.

Tang D, Kang R, Berghe TV, Vandenabeele P, Kroemer G (2019) The molecular machinery of regulated cell death. Cell Res 29:347-364.

Valek L, Häussler A, Dröse S, Eaton P, Schröder K, Tegeder I (2017) Redox-guided axonal regrowth requires cyclic GMP dependent protein kinase 1: Implication for neuropathic pain. Redox Biol 11:176-191.

van Vulpen LF, Roosendaal G, van Asbeck BS, Mastbergen SC, Lafeber FP, Schutgens RE (2015) The detrimental effects of iron on the joint: a comparison between haemochromatosis and haemophilia. J Clin Pathol 68:592-600.

Volkow N, Benveniste H, McLellan AT (2018) Use and misuse of opioids in chronic pain. Annu Rev Med 69:451-465.

Wang F, He J, Xing R, Sha T, Sun B (2021) Molecular mechanisms of ferroptosis and their role in inflammation. Int Rev Immunol 17:1-11.

Wang H, Huo X, Han C, Ning J, Chen H, Li B, Liu J, Ma W, Li Q, Yu Y, Shi K (2021) Ferroptosis is involved in the development of neuropathic pain and allodynia. Mol Cell Biochem 476:3149-3161.

Xu W, Liu W, Yu W (2019) The involvement of iron responsive element (-) divalent metal transporter 1-mediated the spinal iron overload via CXCL10/CXCR3 pathway in neuropathic pain in rats. Neurosci Lett 694:154-160.

Yang Y, Zhao J, Li Y, Li X, Chen X, Feng Z (2021) Fragile X mental retardation protein-regulated proinflammatory cytokine expression in the spinal cord contributes to the pathogenesis of inflammatory pain induced by complete Freund's adjuvant. J Neurochem 159:512-524.

Yao MY, Liu T, Zhang L, Wang MJ, Yang Y, Gao J (2021) Role of ferroptosis in neurological diseases. Neurosci Lett 747:135614.

Yin Y, Yi MH, Kim DW (2018) Impaired autophagy of GABAergic interneurons in neuropathic pain. Pain Res Manag 2018:9185368.

Zhang JJ, Du J, Kong N, Zhang GY, Liu MZ, Liu C (2021a) Mechanisms and pharmacological applications of ferroptosis: a narrative review. Ann Transl Med 9:1503.

Zhang LQ, Zhou YQ, Li JY, Sun J, Zhang S, Wu JY, Gao SJ, Tian XB, Mei W (2022) 5-HT1F receptor agonist ameliorates mechanical allodynia in neuropathic pain via induction of mitochondrial biogenesis and suppression of neuroinflammation. Front Pharmacol 13:834570.

Zhang Y, Swanda RV, Nie L, Liu X, Wang C, Lee H, Lei G, Mao C, Koppula P, Cheng W, Zhang J, Xiao Z, Zhuang L, Fang B, Chen J, Qian SB, Gan B (2021b) mTORC1 couples cyst(e)ine availability with GPX4 protein synthesis and ferroptosis regulation. Nat Commun 12:1589.

Zhao XH, Zhang T, Li YQ (2015) The up-regulation of spinal Toll-like receptor 4 in rats with inflammatory pain induced by complete Freund's adjuvant. Brain Res Bull 111:97-103.

Zheng Z, Tang D, Zhao L, Li W, Han J, Hu B, Nie G, He Y (2020) Liproxstatin-1 protects hair cell-like HEI-OC1 cells and cochlear hair cells against neomycin ototoxicity. Oxid Med Cell Longev 2020:1782659.

Zilka O, Shah R, Li B, Friedmann Angeli JP, Griesser M, Conrad M, Pratt DA (2017) On the mechanism of cytoprotection by ferrostatin-1 and liproxstatin-1 and the role of lipid peroxidation in ferroptotic cell death. ACS Cent Sci 3:232-243.

C-Editor: Zhao M; S-Editor: Li CH; L-Editors: Iwabuchi S, Li CH, Song LP; T-Editor: Jia Y

Additional Table 1 Paw withdrawal threshold values (g) of rats that were administered different volumes of liproxstatin-1

	Time after CFA injection (d)				
	-3	1	3	5	7
Con	19.89±3.79	19.28±2.76	19.00±4.66	19.28±3.60	20.50±3.84
CFA	19.89±3.79	2.32±1.39*	1.73±1.02*	2.19±1.33*	2.45±1.07*
CFA+Veh	23.56±2.99	1.64±0.86*	1.71±1.04*	2.53±1.17*	2.57±1.04*
CFA+Lip-1 (10 μL)	21.11±2.99	2.22±1.01*	2.27±0.92*	3.44±1.67*	4.78±1.71
CFA+Lip-1 (20 μL)	20.50±3.07	2.21±1.24*	3.30±1.33*	3.56±0.91*	5.34±2.23
CFA+Lip-1 (30 μL)	19.89±4.44	1.70±0.82*	5.89±0.88*#	8.00±1.98*#	9.22±0.98*#
CFA+Lip-1 (40 μL)	21.11±3.79	1.88±3.79*	4.32±2.10*	7.17±2.51*#	8.00±2.11*#

At −3 and 1 days after the complete Freund's adjuvant (CFA) injection, there were six rats in each group. Because the intrathecal injection of liproxstatin-1 caused lower limb paralysis in two of the six rats in the CFA+Lip-1 (40 μL) group, the number of rats in this group reduced to four from the third day after CFA injection. Data are expressed as means ± SDs and represent results of three independent experiments in five rats per group. Data were analyzed using a two-way repeated-measures analysis of variance, followed by Bonferroni post hoc tests. *$P < 0.05$, vs. Con group; #$P < 0.05$, vs. CFA+Veh group. CFA: complete Freund's adjuvant; Lip: liproxstatin-1; Veh: vehicle.

Additional Table 2 Paw thermal withdrawal latency (s) of rats that were administered different volumes of liproxstatin-1

	Time after CFA injection (d)				
	-3	1	3	5	7
Con	11.52±1.45	12.42±1.33	13.16±0.99	13.10±1.41	12.23±2.00
CFA	11.88±1.06	5.24±0.62*	5.04±0.51*	5.04±0.96*	5.28±1.16*
CFA+Veh	12.28±1.18	5.10±0.71*	5.16±0.54*	4.87±1.04*	5.08±1.09*
CFA+Lip-1 (10 μL)	12.12±1.18	5.34±0.34*	5.64±0.74*	6.01±0.95*	7.19±0.78*
CFA+Lip-1 (20 μL)	11.71±0.95	4.96±0.50*	6.06±1.19*	6.72±0.51*	7.31±0.62*
CFA+Lip-1 (30 μL)	12.19±1.49	5.50±0.41*	7.21±0.69*#	8.83±0.99*#	9.19±0.99*#
CFA+Lip-1 (40 μL)	11.95±1.42	5.42±0.50*	6.43±1.35*	7.32±0.64*#	8.41±1.12*#

At −3 and 1 days after complete Freund's adjuvant (CFA) injection, there were six rats in each group. Because the intrathecal injection of liproxstatin-1 caused lower limb paralysis in two of the six rats in the CFA + Lip-1 (40 μL) group, the number of rats in this group reduced to four from the third day after CFA injection. Data are expressed as means ± SDs and represent the results of three independent experiments in five rats per group. Data were analyzed using a two-way repeated-measures analysis of variance, followed by Bonferroni post hoc tests. *$P < 0.05$, vs. Con group; #$P < 0.05$, vs. CFA+Veh group. CFA: complete Freund's adjuvant; Lip: liproxstatin-1; Veh: vehicle.